Micromagnetic simulation of Sm–Co/α-Fe/Sm–Co trilayers with various angles between easy axes and the film plane*

Zhang Xi-Chao(张溪超)[a], Zhao Guo-Ping(赵国平)[a]†, Xia Jing(夏 静)[a], Yue Ming(岳 明)[b], Yuan Xin-Hong(袁新红)[a], and Xie Lin-Hua(谢林华)[a]

[a] College of Physics and Electronic Engineering, Sichuan Normal University, Chengdu 610066, China
[b] College of Materials Science and Engineering, Beijing University of Technology, Beijing 100124, China

(Received 16 February 2014; revised manuscript received 13 March 2014; published online 23 July 2014)

Hysteresis loops and energy products have been calculated systematically by a three-dimensional (3D) software OOMMF for Sm–Co/α-Fe/Sm–Co trilayers with various thicknesses and β, where β is the angle between the easy axis and the field applied perpendicular to the film plane. It is found that trilayers with a perpendicular anisotropy possess considerably larger coercivities and smaller remanences and energy products compared with those with an in-plane anisotropy. Increase of β leads to a fast decrease of the maximum energy product as well as the drop of both remanence and coercivity. Such a drop is much faster than that in the single-phased hard material, which can explain the significant discrepancy between the experiment and the theoretical energy products. Some modeling techniques have been utilized with spin check procedures performed, which yield results in good agreement with the one-dimensional (1D) analytical and experimental data, justifying our calculations. Further, the calculated nucleation fields according to the 3D calculations are larger than those based on the 1D model, whereas the corresponding coercivity is smaller, leading to more square hysteresis loops and better agreement between experimental data and the theory.

Keywords: micromagnetic simulation, hard/soft trilayers, hysteresis loops, magnetization configuration

PACS: 75.60.JK, 75.60.Ej, 75.70.Cn, 75.50.Ss **DOI:** 10.1088/1674-1056/23/9/097504

1. Introduction

The concept of an exchange-coupled hard/soft composite nanomagnet was proposed by Kneller *et al.*[1] in 1991, which possesses a large remanence provided by the soft phase and a large coercivity provided by the hard phase.[2–14] Therefore, an energy product much larger than the conventional permanent magnets can be achieved in theory.[15,16] In 1993, Skomski and Coey[17] predicted that the energy product of hard/soft multilayers can be as high as 120 MGOe, which doubles that of the sintered Nd–Fe–B, the best single-phased permanent magnet up to now. Great efforts have been devoted to realize such a giant energy product in the past two decades. Experimental energy products, however, turn out to be much lower than the theoretical one, even smaller than the sintered Nd–Fe–B. An energy product paradox is proposed therefore in some literature, which has been intensively studied in both experimental[18–24] and theoretical[25–31] works by scientists. Further, the price of rare-earth materials rose rapidly in the last few years, which gives the investigation of the composite nanomagnets another push. More economical composites are preferred to the traditional single-phased rare-earth metal compounds.

A detailed review shows that most theoretical works in this field use a simple one-dimensional (1D) micromagnetic model with well-oriented easy axes. Three-dimensional calculations (3D), with a deviation of easy axis from the applied field direction in particular, has seldom been performed.

Deviation of easy axis has been taken into account in Ref. [30], where an angle between easy axes and the applied field H has been assumed in the 1D micromagnetics, with both of them lying in the film plane. It is found that the deviation of easy axes can deteriorate the energy products of $Nd_2Fe_{14}B$/α-Fe significantly.

Experimentally, major progress has been made in the last year,[21] where an energy product of 60 MGOe has been achieved in Nd–Fe–B/Fe–Co multilayers by Cui *et al.*[21] Such a high energy product surpasses that of the best single-phased Nd–Fe–B already, which, interestingly, is realized with a perpendicular crystalline anisotropy rather than with a parallel one.

Besides Nd–Fe–B/Fe and Nd–Fe–B/Fe–Co systems, Sm–Co/Fe systems have aroused much interest recently.[18,32,33] Sm–Co is the hardest material in the world which can provide the largest possible coercivity whilst the large remanence can be retained by α-Fe. In particular, the compound Fe–Co with a very high saturation magnetization of 1.93×10^3 emu/cc, can be formed spontaneously at the interface to improve the rema-

*Project supported by the National Natural Science Foundation of China (Grant Nos. 11074179, 10747007, 51331003, 51371011, and 51001002), the State Key Development Program of Basic Research of China (Grant No. 2010CB934600), the Construction Plan for Scientific Research Innovation Teams of Universities in Sichuan Province, China (Grant No. 12TD008), the Beijing Municipal Natural Science Foundation, China (Grant No. 2122006), and Scientific Research Innovation Fund for Student in Sichuan Normal University, China.

†Corresponding author. E-mail: zhaogp@uestc.edu.cn; zapple2004@yahoo.com

© 2014 Chinese Physical Society and IOP Publishing Ltd

nence and the energy product significantly.

Choi *et al.*[8] found that the maximum energy product of Sm–Co/Fe bilayers can be improved by 50% with an intermixed interface layer. Zhang *et al.*[34] found that the addition of Cu in $SmCo_5$/Fe multilayers can significantly increase the BH_{max} from 9 MGOe to 32 MGOe. The largest energy product for Sm–Co/Fe reported so far is around 40 MGOe, achieved by Sawatzki *et al.*[33] in $SmCo_5$/Fe/$SmCo_5$ trilayers, where an interface Fe–Co layer is formed which significantly improves the $(BH)_{max}$. These superior energy products have been achieved with a well-oriented in-plane easy axis, as predicted by the present micromagnetic theory.

In this paper, three-dimensional (3D) micromagnetic simulations have been performed for Sm–Co/α-Fe/Sm–Co trilayers, using the object oriented micromagnetic framework (OOMMF)[35] software. The calculation is started with a perpendicular anisotropy and compared carefully with the 1D calculations to see whether a perpendicular anisotropy is favored over an in-plane one in achieving excellent magnetic properties. Our 3D simulations focus on the influence of an out-of-plane deviation of easy axis β, which is the angle between the crystalline easy axis and the applied field.

2. Micromagnetic model

The trilayer system studied in this paper is shown in Fig. 1, where a soft layer is sandwiched between two hard layers with the applied field perpendicular to the plane. The easy axis, on the other hand, can change continuously from the perpendicular to the parallel direction defined relative to the film plane. The angle β between the applied field and the easy axis, as a result, varies between 0° and 90° in this simulation.

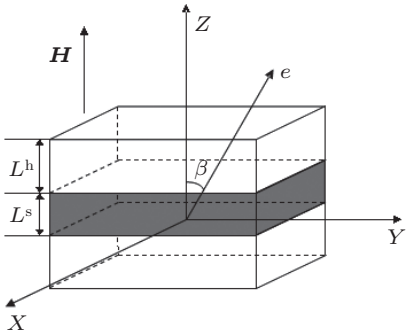


Fig. 1. The basic scheme for a three-dimensional micromagnetic model of the hard/soft/hard trilayer.

The 3D simulation performed by OOMMF is based on the Landau–Lifshitz–Gilbert (LLG) dynamic equation

$$\frac{\mathrm{d}\boldsymbol{M}}{\mathrm{d}t} = \frac{-\omega}{1+\alpha^2}\boldsymbol{M}\times\boldsymbol{H}_{\mathrm{eff}} - \frac{\alpha\omega}{(1+\alpha^2)M_{\mathrm{S}}}\boldsymbol{M}\times(\boldsymbol{M}\times\boldsymbol{H}_{\mathrm{eff}}), \quad (1)$$

where $\boldsymbol{M}$ is the magnetization, $\boldsymbol{H}_{\mathrm{eff}}$ is the effective field, ω is the gyromagnetic ratio, and α is the damping coefficient. The relaxation time of the system depends on the damping coefficient α, which is typically in the range 0.004 to 0.15 for physical materials. Since it has no impact on the equilibrium state of the system, we set the value of α as 0.5 to allow the solver to converge in a reasonable number of iterations. Meanwhile, the value for ω is 2.211×10^5, which is a default value here.

The effective field is defined as follows:

$$\boldsymbol{H}_{\mathrm{eff}} = -\mu_0^{-1}\frac{\partial E}{\partial \boldsymbol{M}}. \quad (2)$$

The average energy density E is a function of $\boldsymbol{M}$ specified by Brown's equations,[36] including the exchange, the anisotropy, the applied field (Zeeman) and the magnetostatic (demagnetization) terms.

In the 3D simulation, the trilayer system is set as a tetragonal box, 300 nm × 300 nm × L, where L equals $2L^{\mathrm{h}}+L^{\mathrm{s}}$ as shown in Fig. 1. The thickness of the hard layer L^{h} keeps a constant value of 10 nm, while that of the soft layer L^{s} varies between 2 nm and 10 nm. The trilayer magnetic structure is discretized into lattice cells with the same cell size of 3 nm × 3 nm × 1 nm, which has been optimized between calculation accuracy and computational time. The reliability of the calculation is guaranteed by performing the spin check to make sure that the maximum angle between neighboring spins in the simulation is less than 30 degrees.

The applied field varies from 6 T to −6 T in the simulation, starting from a positive saturation state, where the magnetic moment is uniformly distributed and the micromagnetic structure distribution thereafter could be derived from the LLG equation. Only the exchange interaction between the neighboring region pair is taken into account and the free boundary conditions are chosen.

In this paper, Sm–Co is chosen as the hard layer while α-Fe is the soft layer. The material parameters for the simulation are adopted from Refs. [25] and [37], which are (in CGS units): $M_{\mathrm{s}}^{\mathrm{s}} = 1.7\times10^3$ emu/cc, $M_{\mathrm{s}}^{\mathrm{h}} = 5.5\times10^2$ emu/cc, $K^{\mathrm{s}} =$ 1000 erg/cc, $K^{\mathrm{h}} = 5\times10^7$ erg/cc, $A^{\mathrm{s}} = 2.8\times10^{-6}$ erg/cm, $A^{\mathrm{h}} = 1.2\times10^{-6}$ erg/cm, and $A^{\mathrm{hs}} = 1.8\times10^{-6}$ erg/cm. Here, A, K, and M_{s} denote the exchange energy constant, the anisotropy constant, and the spontaneous magnetization, respectively. The superscripts h and s refer to the hard and soft layers, respectively.

In the real simulation process, the case where β equals exactly 0° might get stuck on non-stable equilibrium states and hence to produce overly large coercive values.[38] This problem can be overcome by adding an activation source such as a non-zero temperature effect in the simulation. In the present work, a tilting angle of 0.5° between the easy axis and the applied field has been utilized to mimic the case where β equals exactly 0°. Therefore, in the following, all the cases with $\beta = 0°$ refer to the corresponding cases with such a slight tilting angle.

3. Calculated hysteresis loops and coercivities

Figure 2 shows the calculated hysteresis loops for Sm–Co/α-Fe trilayers with various β, where the thicknesses of the hard and soft layers are set as $L^{\rm h} = 10$ nm and $L^{\rm s} = 2$ nm. It can be seen that the shapes of the hysteresis loops are quite sensitive to the value of β. As β increases, the hysteresis loop becomes more slanted, accompanied by an obvious decrease of the remanence.

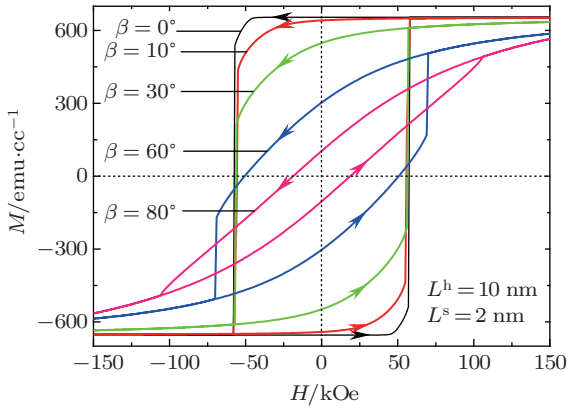


Fig. 2. (color online) Macroscopic hysteresis loops of the Sm–Co (10 nm)/α-Fe (2 nm)/Sm–Co (10 nm) trilayers with various values of β, where β is the angle between the easy axis and the applied field.

When $\beta = 0°$, the shape of the hysteresis loop is basically a rectangle, with a remanence of 654.8 emu/cc, which equals the saturation magnetization, the largest possible value of the remanence for the Sm–Co (10 nm)/α-Fe (2 nm)/Sm–Co (10 nm) trilayers. There is an obvious nucleation point near the applied field of -50 kOe and a clear-cut pinning point at $H = -57.3$ kOe. Before the nucleation point, all the magnetization in the system orient parallel to the z axis, the direction of the previous saturation state, so that this part of the curve is a horizontal line parallel to the H axis as shown in Fig. 2. At the pinning point, the irreversible magnetization reversal takes place, which sweeps throughout the whole system and helps the system to pass the coercive point. The curve at this critical state is a vertical line parallel to the M axis.

When $\beta \neq 0°$, the complete saturation state cannot be reached and hence no obvious nucleation point exists. Therefore, no part of the loop is exactly horizontal, and the loop at a very large applied field, can only say to approach the horizontal line. Nevertheless, a clear-cut pinning point still exists to form a vertical part of the hysteresis loop. However, the magnetization of the system does not reverse completely at the pinning point. Instead, it reaches a state near 180°, leaving a space for a gradual process approaching to saturation. The remanence of the system decreases monotonically from 654.8 emu/cc to 103.8 emu/cc as β increases from 0° to 80° and will decrease to 0 emu/cc when $\beta = 90°$ according to the Stoner–Wohlfarth (SW) model.[39] It is noted that the calculated remanence is slightly smaller than $M_{\rm S}\cos\beta$[40] due to the deterioration effect of the stray fields, where the $M_{\rm S}$ is the saturation magnetization of the composite system. For example, the remanence for $\beta = 30°$ is 548.3 emu/cc, whereas the remanence according to $M_{\rm S}\cos 30°$ is 566.8 emu/cc.

For a small β, the coercivity equals the pinning field so that the dominant coercivity mechanism is pinning. For $\beta < 45°$, both the coercivity and the pinning field roughly keep a constant value of 57 kOe. For larger β, the coercivity deviates from the pinning field. As β increases from 50° to 80°, the pinning field increases from 62 kOe to 106 kOe, whereas the coercivity decreases from 60 kOe to 19 kOe. The pinning field will reach a maximum at $\beta = 90°$ while the corresponding coercivity decreases to 0.

Figure 3 shows the hysteresis loops for various β with $L^{\rm s} = L^{\rm h} = 10$ nm. Similar to Fig. 2, the increment of β will lead to the significant reduction of the remanence and coercivity as well as the increase of the pinning field. Compared with Fig. 2, the hysteresis loops in Fig. 3 are much slimmer due to the smaller pinning field and the coercivity while the remanence of the system decreases faster with the rising β. The maximum remanence is 777.8 emu/cc obtained at $\beta = 0°$, while the coercivity reaches its maximum value of 25.9 kOe at $\beta = 20°$. More details of hysteresis loops are shown in Table 1.

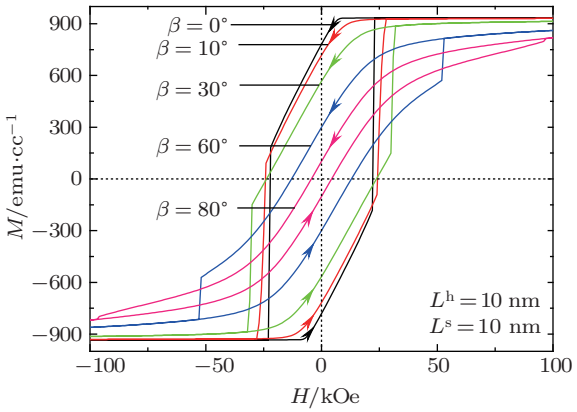


Fig. 3. (color online) Macroscopic hysteresis loops of the Sm–Co (10 nm)/α-Fe (10 nm)/Sm–Co (10 nm) trilayers with various values of β, where β is the angle between the easy axis and the applied field.

Figure 4 shows the change of the coercivity with the easy axis deviation for three different $L^{\rm s}$ where the thickness of the hard layer keeps a constant value of 10 nm. For $L^{\rm s} = 2$ nm, the coercivity is roughly a constant as β increases from 0° to 50°, with a shallow valley ($H_{\rm c} = 55$ kOe) around $\beta = 20°$. The coercivity drops fast for larger β, so that a peak value of 60 kOe emerges at $\beta = 50°$. A similar trend can be observed for other values of $L^{\rm s}$, where the peak values correspond to 40° and 20° for $L^{\rm s} = 5$ nm and $L^{\rm s} = 10$ nm respectively.

The coercivity reduces to zero at $\beta = 90°$, no matter how thick is the soft layer. On the other hand, for a given β, the coercivity decreases uniformly with the soft layer thickness. Similar results have been obtained by Xia *et al.* for a hard/soft trilayer with an in-plane deviation of the easy axis.[30]

Table 1. Characteristic values in the calculated hysteresis loops for a Sm–Co (10 nm)/α-Fe (L^s)/Sm–Co (10 nm) trilayer, where M_r, H_c, and H_p are the remanence, coercivity, and pinning field respectively.

	M_r/emu·cc^{-1}			H_c/kOe			H_p/kOe		
β	2 nm	5 nm	10 nm	2 nm	5 nm	10 nm	2 nm	5 nm	10 nm
0°	654.8	779.8	777.8	57.3	33.3	22.2	57.3	33.3	22.2
10°	641.5	738.8	717.0	55.7	34.3	24.2	55.7	34.3	24.2
20°	604.6	670.6	644.3	55.4	36.2	25.9	55.4	36.2	26.1
30°	548.3	592.8	566.2	56.3	39.1	23.8	56.3	39.1	29.8
40°	477.2	507.0	482.6	58.1	39.9	20.6	58.1	43.0	35.1
50°	394.7	414.5	392.8	59.9	34.4	16.9	62.0	48.1	41.0
60°	302.9	315.5	299.1	50.6	26.8	12.9	69.1	58.0	52.1
70°	205.2	212.9	201.3	36.1	18.2	8.6	82.0	73.2	68.2
80°	103.8	107.4	101.1	18.7	9.3	4.4	105.8	100.9	96.6

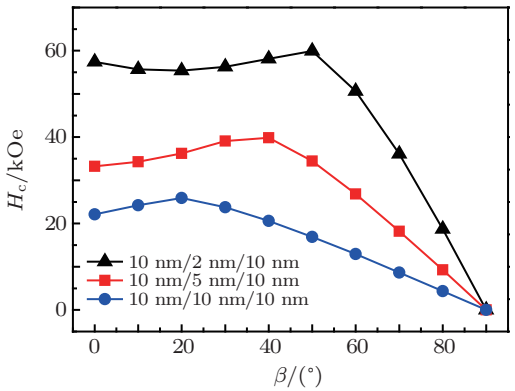


Fig. 4. (color online) Dependence of the coercivity on the easy axis deviation β for various soft layer thickness with a fixed hard layer of 10 nm.

4. Comparison between 3D and 1D hysteresis loops

Our calculation is in good agreement with those calculated by the 1D model,[28,30] as demonstrated in Fig. 5 for $\beta = 0°$. The best agreement can be obtained when $L^s = 2$ nm, where the remanences by both models are equal to 654.8 emu/cc with close nucleation and pinning points, justifying our calculation. A fine comparison shows that the nucleation field according to the 3D calculation is larger whereas the pinning field is smaller. Both models indicate that the coercivity mechanism is pure pinning, where the coercivity equals exactly to the pinning field. The difference for the nucleation fields is due mainly to the different nucleation modes revealed, i.e., the curling modes according to the 3D calculation and the quasi-coherent modes assumed in the 1D model.[41] On the other hand, the small coercivity difference between 1D and 3D calculations is due to the unavoidable stray fields, which are ignored in the 1D calculation.

The above discussion holds for other values of L^s, where nucleation occurs later according to the 3D calculation whereas the depinning occurs slightly earlier. These differences lead to more square hysteresis loops and hence better agreement between the theory and the experiment. As the soft layer thickness rises, both nucleation and pinning fields decrease. In the meantime, the calculated difference between 1D and 3D coercivities goes up, accompanied by the enlargement of the gap between the calculated nucleation and pinning fields. The coercivity mechanism according to both models is pure pinning when L^s equals 2 nm and 5 nm. For $L^s = 10$ nm, however, the coercivity mechanism based on the 3D model is still pure pinning, whereas that according to the 1D model is in-between the nucleation and pinning, where the coercivity is slightly smaller than the pinning field.

The inset of Fig. 5 compares the L^s-dependent coercivity calculated by 1D and 3D models for $L^h = 10$ nm and $\beta = 0°$. For small soft layer thickness ($L^s = 2$ nm), the coercivities based on 1D and 3D models are very close, justifying our calculation. The calculated difference goes up to 4 kOe when L^s increases to 5 nm. This difference (4 kOe) holds for larger values of L^s.

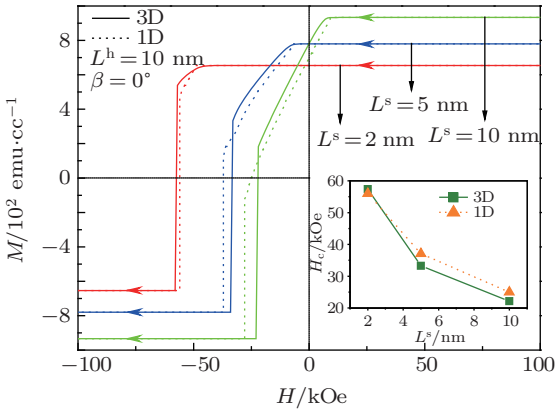


Fig. 5. (color online) Comparison of 1D (dashed line) and 3D (solid line) calculated hysteresis loops for Sm–Co (10 nm)/α-Fe/Sm–Co (10 nm) with various soft layer thickness and $\beta = 0°$. The inset compares the calculated coercivity.

5. Calculated magnetic moment distributions

Figure 6 shows the calculated magnetization configurations in the y–z plane for a Sm–Co (10 nm)/α-Fe (10 nm)/Sm–Co (10 nm) trilayer with easy axis perpendicular to the film plane. The magnetic moments in both phases align exactly with the applied field when the absolute value of the applied field is large ($H > 25$ kOe), which are not drawn in the fig-

ure. At $H = -9$ kOe, a middle point between nucleation and pinning, obvious deviation of the magnetic moments from the previous saturation direction can be observed inside the α-Fe layer. However, those within the Sm–Co layers have only a slight deviation, due to its large crystalline anisotropy. Magnetic moments inside the α-Fe layer respond to the applied field fast, which then drags the moments within the Sm–Co layers to follow this response through the exchange interaction. When the applied field decreases to -22 kOe, the magnetic moments inside the α-Fe layer have reversed already. In the meantime, obvious deviation of the magnetization orientation can be found within the Sm–Co layers near the interface due to the drive of the magnetization in the α-Fe layer, whereas those at the surfaces still orient near the previous saturation direction. As a result, a 110° domain wall is formed, which crosses the two phases. Further decrease of the applied field will lead to the complete reversal of the whole system.

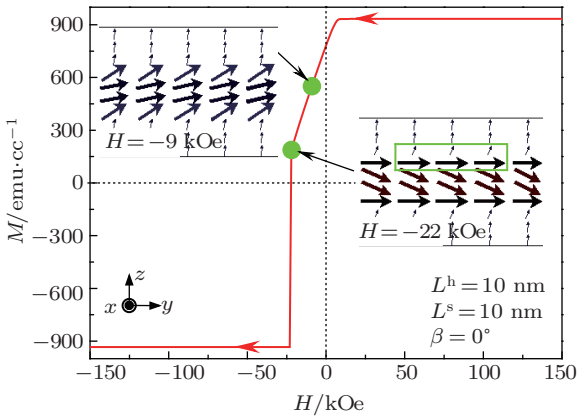


Fig. 6. (color online) Simulated magnetization configurations within the y–z plane (perpendicular to the film plane) for a Sm–Co (10 nm)/α-Fe (10 nm)/Sm–Co (10 nm) trilayer with $\beta = 0°$ along with the calculated hysteresis loops. The small and large arrows denote the magnetic moments within the Sm–Co and α-Fe layers respectively. The green box encloses the interface spins, which orients right at the film plane at a field of -22 kOe.

Figure 7 shows the calculated magnetization configurations for a Sm–Co (10 nm)/α-Fe (10 nm)/Sm–Co (10 nm) trilayer with $\beta = 50°$. For any β in between 0° and 90°, the magnetizations cannot align to the applied field direction no matter how large is the applied field and hence the name approaching to saturation, which is quite different from those shown in Fig. 6. When $H = 100$ kOe, the magnetic moments in the α-Fe layer have only a slight deviation from the applied field direction due to its tiny crystalline anisotropy, whereas those in the Sm–Co layers exhibit an obvious deviation already at such a huge applied field. As mentioned before, the magnetizations in the soft layer respond to the applied field fast and drag those in the hard layers through the exchange coupling. At $H = -9$ kOe, the spins in the α-Fe layer rotate roughly 90° away from the applied field direction, whereas those in Sm–Co layers have a deviation about 60° only. At $H = -41$ kOe, spins inside the hard phase display a difference in response to the applied field. Those near the interface deviate 85° away from the previous saturation direction whereas those near the surfaces retain a 62° deviation. On the other hand, the spins within the soft phase have reversed already, forming a 90° domain wall. This state is a critical state, i.e., pinning point of the system. Further decrease of the applied field will lead to the depinning of the domain wall and irreversible rotation of the spins in the whole system, leading to a vertical part in the hysteresis loop. However, the magnetic orientations do not jump to 180° as shown in Fig. 6. Instead, the spins in the soft and hard layers jump to respectively, 190° and 230°, which is consistent with the SW model. According to the SW model, they jump to 213° after the magnetic reversal.

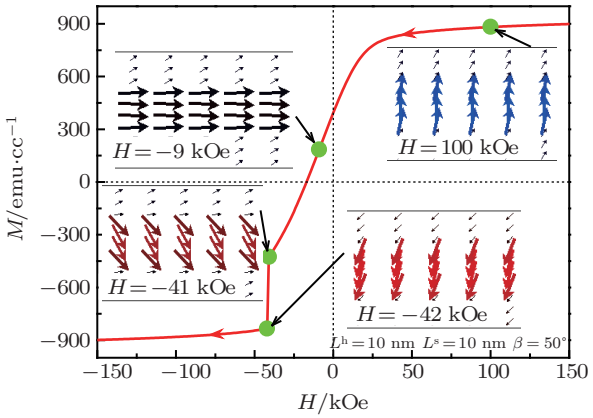


Fig. 7. (color online) Simulated magnetization configurations within the y–z plane for Sm–Co (10 nm)/α-Fe (10 nm)/Sm–Co (10 nm) with $\beta = 50°$ along with the calculated hysteresis loops. The small and large arrows denote the magnetic moments within the Sm–Co and α-Fe layers respectively.

6. Calculated energy products and discussion

Figure 8 shows the calculated energy products for Sm–Co (10 nm)/α-Fe (2 nm)/Sm–Co (10 nm) trilayers with various β, which is very sensitive to the deviation angle β. Similar sensitivity has been found in the hard/soft trilayer with an in-plane deviation of the easy axis.[30] A $(BH)_{max}$ of 16.9 MGOe is found in an oriented trilayer ($\beta = 0°$), which decreases to 16.2 MGOe (drops by 4.3%) for a slight deviation of the easy axis ($\beta = 10°$). Further deviation leads to a fast decrease of the maximum energy product. As shown in Fig. 8, BH_{max} reduces to 8.6 MGOe (drops by 50%) when $\beta = 40°$ and declines to 0.3 MGOe when β increases to 80°. Such a tremendous decrease of the maximum energy product with the deviation of the easy axis explains the significant discrepancy between experimental and theoretical energy products well.

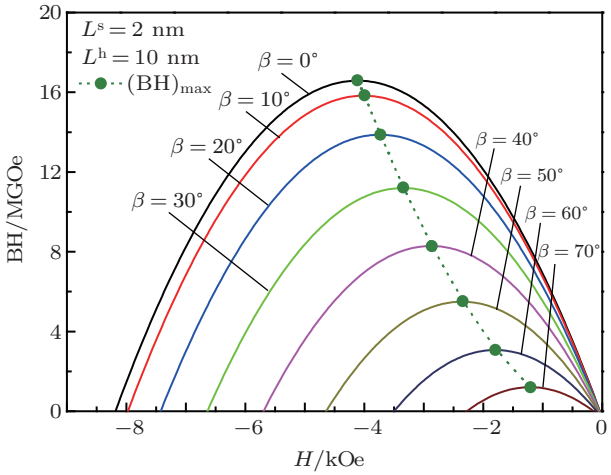


Fig. 8. (color online) Calculated second-quadrant energy products for Sm–Co (10 nm)/α-Fe (2 nm)/Sm–Co (10 nm) with various β.

Similar results exist for other values of L^s, as demonstrated in Table 2. The maximum energy products fall fast with the increases of β, especially for large soft layer thickness. The largest $(BH)_{max}$ is about 24 MGOe, obtained at $L^s = 5$ nm with $\beta = 0°$, which is about twice that for single-phased Sm–Co magnets. The maximum energy product decreases to 20 MGOe (drops by 17%) at a β of 10° and declines to 12 MGOe (drops by 49%) at $\beta = 30°$. This drop is much faster than that for the single-phased Sm–Co magnets, where the maximum energy product drops by 26% only at $\beta = 30°$. Therefore, the advantage of the composite magnets is realized only when they are well oriented.

Table 2. Comparison of the maximum energy products for single phased Sm–Co magnets and Sm–Co (10 nm)/α-Fe/Sm–Co (10 nm) trilayers.

β	$(BH)_{max}$/MGOe			
	Single-phased	L^s = 2 nm	L^s = 5 nm	L^s = 10 nm
0°	11.94	16.90	23.95	18.20
10°	11.57	16.17	19.95	15.39
20°	10.50	14.14	16.11	12.72
30°	8.87	11.42	12.33	9.79
40°	6.90	8.62	8.99	6.99
50°	4.82	5.71	5.89	4.74
60°	2.91	3.38	3.38	2.47
70°	1.35	1.52	1.53	1.24
80°	0.34	0.24	0.20	0.00

Our calculated energy products are in reasonable agreement with most experimental data. Most experimental energy products for Sm–Co/Fe are between 10 MGOe and 20 MGOe if the easy axis orientation is quite good and below 10 MGOe otherwise. For example, Choi *et al.*[8] fabricated Sm–Co/Fe bilayers with the energy products ranging from 10 MGOe to 15 MGOe. Similar results have been found by Fullerton *et al.*[37] On the other hand, Zhang *et al.*[34] found that the largest BH_{max} is achieved when the thicknesses of the hard and soft layers are 9 nm and 5 nm respectively, consistent with our results shown in Table 2. However, the energy products of 40 MGOe and 32 MGOe achieved by Sawatzki *et al.*[33] and Zhang *et al.*[34] respectively, are obviously too high to be explained by the present modeling with a perpendicular anisotropy. These deviations come from the different easy axis orientation, apart from the formation of the Fe–Co interlayer and additions of Cu in the respective experiments.

To explain the high energy products mentioned above, we have performed 3D calculations for Sm–Co/α-Fe/Sm–Co trilayers with in-plane easy axes. Table 3 shows the characteristic values in the calculated hysteresis loops for Sm–Co (10 nm)/α-Fe (10 nm)/Sm–Co (10 nm) with various in-plane deviations of the easy axis β'. It can be seen that the calculated energy products in Table 3 are consistent with those reported in Refs. [33] and [34]. Further, the calculated coercivities with in-plane easy axes are systematically smaller than those with a perpendicular anisotropy whereas the remanences are systematically larger. Similar trends have been found in Nd–Fe–B/Fe, Nd–Fe–B/Fe–Co and other compounds. The coercivities in Sm–Co/Fe are large enough to obtain a maximum energy product so that the energy products are determined mainly by the remanence in Sm–Co/Fe multilayers, which explains why the superior energy products are achieved in Sm–Co/Fe multilayers with an in-plane rather than with a perpendicular anisotropy. For Nd–Fe–B/Fe and Nd–Fe–B/Fe–Co multilayers, however, the experimental coercivity is usually smaller than the necessary one to achieve a maximum energy product due to the famous Brown's coercivity paradox.[36] Therefore, the outstanding data for energy products used to appear in the materials with a perpendicular anisotropy.

Table 3. Characteristic values in the calculated hysteresis loops for a Sm–Co (10 nm)/α-Fe (10 nm)/Sm–Co (10 nm) trilayer with in-plane easy axis deviations, where M_r, H_c, and H_p are the remanence, coercivity and pinning field respectively.

β'	M_r/emu·cc^{-1}	H_c/kOe	H_p/kOe	$(BH)_{max}$/MGOe
0°	933.8	15.4	15.4	34.2
10°	917.5	18.1	18.1	31.1
20°	871.5	18.2	20.0	25.5
30°	801.9	16.5	25.0	19.9
40°	707.1	14.2	31.0	14.4
50°	589.8	11.7	40.0	9.2
60°	459.0	8.8	52.9	5.5

7. Conclusions

In conclusion, the hysteresis loops and magnetization behaviors of Sm–Co/α-Fe/Sm–Co trilayer system for various soft layer thicknesses, have been investigated in detail using the 3D micromagnetic software package OOMMF. The calculation is focused on the influence of the out-of-plane easy axis deviation β, started with a perpendicular crystalline anisotropy.

Both calculated remanence and energy products decrease uniformly as β increases, where $(BH)_{max}$ is very sensitive to

the deviation of the easy axis, especially for large soft layer thickness. The largest $(BH)_{max}$ is 24 MGOe, achieved at $L^s = 5$ nm with $\beta = 0°$. The calculated coercivities and the pinning fields equal each other for small β, which do not change much with the value of β, indicating that the dominant coercivity mechanism is pinning. For large β, however, the coercivity decreases fast whereas the pinning fields increase as β increases. The nucleation occurs later according to the 3D calculation whereas the depinning occurs slightly earlier, leading to better squareness in the hysteresis loops compared with 1D results.

The simulated magnetization configurations clearly display that the magnetic moments within the soft phase respond to the applied field fast, which have completed a partial reversal already and formed a mature domain wall crossing the two phases before the pinning point. The whole system completes its magnetic reversal at the pinning point, leading to a vertical part in the hysteresis loop and approaches the saturation gradually.

In addition, a modeling technique with a slight tilting angle has been utilized with spin check procedures performed, which yield results in good agreement with 1D analytical and experimental data, justifying our calculations.

Acknowledgments

The authors wish to thank Dr. Michael J. Donahue from Mathematical & Computational Sciences Division, NIST for giving valuable advice and suggestion about symmetry breaking problems that helped to improve the micromagnetic simulation. The authors also would like to thank Dr. Liu Xiao-Xi from Department of Information Engineering, Shinshu University for giving useful simulation advice.

References

[1] Kneller E F and Hawig R 1991 *IEEE Trans. Magn.* **27** 3588
[2] Shindo M, Ishizone M, Sakuma A, Kato H and Miyazaki T 1997 *J. Appl. Phys.* **81** 4444
[3] Sabiryanov R F and Jaswal S S 1998 *Phys. Rev. B* **58** 12071
[4] Liu J P, Liu Y, Skomski R and Sellmyer D J 1999 *IEEE Trans. Magn.* **35** 3241
[5] Skomski R, Liu J P and Sellmyer D J 1999 *Phys. Rev. B* **60** 7359
[6] Guo Z J, Jiang J S, Pearson J E, Bader S D and Liu J P 2002 *Appl. Phys. Lett.* **81** 2029
[7] Liu W, Zhang Z D, Liu J P, Chen L J, He L L, Liu Y, Sun X K and Sellmyer D J 2002 *Adv. Mater.* **14** 1832
[8] Choi Y, Jiang J S, Pearson J E, Bader S D, Kavich J J, Freeland J W and Liu J P 2007 *Appl. Phys. Lett.* **91** 072509
[9] Liu Y, Wu Y Q, Kramer M J, Choi Y, Jiang J S, Wang Z L and Liu J P 2008 *Appl. Phys. Lett.* **93** 192502
[10] Hou H C, Liao J W, Lin M S, Lin H J, Chang F H, Chen R Z, Chiu C H and Lai C H 2011 *J. Appl. Phys.* **109** 07C104
[11] Amato M, Pini M G and Rettori A 1999 *Phys. Rev. B* **60** 3414
[12] Fang W and Hong X X 2014 *Chin. Phys. B* **23** 036802
[13] Jia L Y, Yin J H and Ma X Q 2014 *Chin. Phys. B* **23** 027501
[14] Wang Y, Wang R, Xie H L, Bai J M and Wei F L 2013 *Chin. Phys. B* **22** 68506
[15] Papusoi C, Srinivasan K and Acharya R 2011 *J. Appl. Phys.* **110** 083908
[16] Poudyal N and Liu J P 2013 *J. Phys. D: Appl. Phys.* **46** 043001
[17] Skomski R and Coey J M D 1993 *Phys. Rev. B* **48** 15812
[18] Kopte M, Sawatzki S, Schultz L and Neu V 2011 *IEEE Trans. Magn.* **47** 3736
[19] Alexandrakis V, Niarchos D, Tsiaoussis I and Panagiotopoulos I 2008 *J. Magn. Magn. Mater.* **320** 1020
[20] Rong C B, Zhang Y, Kramer M J and Liu J P 2011 *Phys. Lett. A* **375** 1329
[21] Cui W B, Takahashi Y K and Hono K 2012 *Adv. Mater.* **24** 6530
[22] Knutson S J, Shen Y, Horwath J C, Barnes P and Chen C H 2011 *J. Appl. Phys.* **109** 07A762
[23] Yuan F T, Hsiao S N, Liao W M, Chen S K and Yao Y D 2006 *J. Appl. Phys.* **99** 08E915
[24] Tang J, Yang L R, Wang X J, Zhang L, Wei C F, Chen B W and Mei Y 2012 *Acta Phys. Sin.* **61** 240701 (in Chinese)
[25] Asti G, Solzi M, Ghidini M and Neri F M 2004 *Phys. Rev. B* **69** 174401
[26] Asti G, Ghidini M, Pellicelli R, Pernechele C, Solzi M, Albertini F, Casoli F, Fabbrici S and Pareti L 2006 *Phys. Rev. B* **73** 094406
[27] Zhao G P and Wang X L 2006 *Phys. Rev. B* **74** 012409
[28] Zhao G P, Zhao M G, Lim H S, Feng Y P and Ong C K 2005 *Appl. Phys. Lett.* **87** 162513
[29] Belemuk A M and Chui S T 2011 *J. Appl. Phys.* **109** 093909
[30] Xia J, Zhao G P, Zhang H W, Cheng Z H, Feng Y P, Ding J and Yang H T 2012 *J. Appl. Phys.* **112** 013918
[31] Belemuk A M and Chui S T 2011 *J. Appl. Phys.* **110** 073918
[32] Li L L and Bao J C 2011 *Chin. Phys. B* **20** 127502
[33] Sawatzki S, Heller R, Mickel C, Seifert M, Schultz L and Neu V 2011 *J. Appl. Phys.* **109** 123922
[34] Zhang J, Takahashi Y K, Gopalan R and Hono K 2005 *Appl. Phys. Lett.* **86** 122509
[35] Donahue M J and Porter D G 1999 *OOMMF user's guide, version* 1.0. *NISTIR* 6376 National Institute of Standards and Technology, Gaithersburg, MD
[36] Brown W F, Jr 1945 *Rev. Mod. Phys.* **17** 15
[37] Fullerton E E, Jiang J S, Grimsditch M, Sowers C H and Bader S D 1998 *Phys. Rev. B.* **58** 12193
[38] Hillebrands B and Ounadjela K 2003 *Spin Dynamics in Confined Magnetic Structures II* (Berlin: Springer)
[39] Stoner E C and Wohlfarth E P 1948 *Phil. Trans. R. Soc.* **240** 599
[40] At the remanent state, all the magnetizations orient at the easy axis direction, with the remanence given by: $M_r = (L^h M_s^h + L^s M_S^s/2)\cos\beta/(L^h + L^s/2)$
[41] Chen B Z, Zhao G P, Zhang H W and Zhong Z Y 2012 *Physica B: Conden. Matter* **407** 4574